

1 **Understanding model crude oil component interactions on**
2 **kaolinite silicate and aluminol surfaces: towards improved**
3 **understanding of shale oil recovery**

4 **Shansi Tian^{1,2,3}, Valentina Erastova⁴, Shuangfang Lu^{1,2*}, H. Chris Greenwell^{3*},**
5 **Thomas R. Underwood³, Haitao Xue^{1,2}, Fang Zeng², Guohui Chen^{1,2}, Chunzheng**
6 **Wu^{1,2}, Rixin Zhao^{1,2}**

7 ¹ Research Institute of Unconventional Petroleum and Renewable Energy (RIUP&RE),
8 China University of Petroleum (East China), Qingdao 266580, Shandong, PR China

9 ² School of Geosciences, China University of Petroleum (East China), Qingdao 266580,
10 Shandong, PR China

11 ³ Department of Earth Science, Durham University, Durham, DH1 3LE, United
12 Kingdom

13 ⁴ Department of Chemistry, Durham University, Durham, DH1 3LE, United Kingdom

14 ***Corresponding authors:**

15 **Prof. Shuangfang Lu**

16 Research Institute of Unconventional Petroleum and Renewable Energy
17 (RIUP&RE), China University of Petroleum (East China), Qingdao, Shandong, China

18 Phone (or Mobile) No.: +86-18661856596

19 Email: lushuangfang@upc.edu.cn

20 **Prof. H. Chris Greenwell**

21 Department of Earth Science, Durham University, Durham, United Kingdom

22 Durham University, South Road, Durham, DH1 3LE

23 Phone (or Mobile) No.: +44-01913342324

24 Email: chris.greenwell@durham.ac.uk

25 **ABSTRACT:** Shale oil is currently of interest for unconventional resource exploration
26 and development. Understanding the mechanism of interaction between the complex
27 mixture of organic compounds in shale oil and minerals making up the reservoir rock-
28 oil interface will assist recovery. In this study, molecular dynamics simulation is used
29 to study the adsorption characteristics of a model oil mixture within nanoscale intra-
30 particle pores of kaolinite minerals, which form pore filling structures in shale rock. To
31 better understand the effects of oil composition, temperature and pressure on the
32 adsorption properties of the model oil mixture, a range of temperatures (298 K, 323 K,
33 348 K and 373 K) and pressures (1 bar, 50 bar, 100 bar and 200 bar) representing up to
34 reservoir conditions were used. This study shows that adsorption and arrangement of
35 oil molecules is dependent on the surface of kaolinite and the distance away from it.
36 The simulations show polar compounds are likely to be adsorbed on aluminol kaolinite
37 basal surfaces, while alkanes preferentially adsorb on silicate surfaces. In addition, the
38 number of oil molecule bound layers, and total adsorption amount on the silicate surface
39 is greater than the aluminol surface. The density of adsorbed oil is reduced with increase
40 in temperature, while the effect of pressure is not as significant. On the basis of
41 performed molecular simulations, we show the adsorption rate of shale oil on the
42 surfaces of kaolinite sheets and assess the removable capacity of the model oil.

43 **Keywords:** shale oil, molecular dynamics, clay mineral, recovery.

44 1. INTRODUCTION

45 With increasing demand for energy, and while conventional oil and gas resources are
46 depleting, unconventional oil and gas are receiving more attention as they have become
47 a major contributor to sustained growth in global hydrocarbon production. The
48 exploration and development of shale gas has achieved notable success in North
49 America,¹⁻³ and led a global shale gas research boom.^{4,5} However, with the lessons
50 learned from initial phases of shale gas extraction and the decrease of natural gas price,
51 investors have now shifted their attention to more profitable shale oil.⁶⁻⁸ According to
52 the Energy Information Administration,⁹ in the last 10 years, the production of U.S.
53 shale oil has increased 12.2 times to an average of 4.57 million barrels per day
54 (MMbbl/d) in 2015, compared to 0.37 MMbbl/d in 2005. Driven by the exploitation of
55 tight sand formations, the United States remained the world's top producer of petroleum
56 and natural gas hydrocarbons in 2015.¹⁰ Shale oil is playing a significant role in the
57 global energy industry, and a worldwide shale-oil boom is predicted.¹¹⁻¹³

58 Preliminary evaluation has shown that shale oil resources are very rich in China,
59 with the amount of geological resources put at 32 billion barrels, and China ranked third
60 among the 41 countries which have an accumulated total shale oil resource of 345
61 billion barrels.¹⁴ At present, in China, a number of reserves in which the amount of
62 geological resources are between 3.5×10^9 barrels and 7×10^9 barrels have been
63 discovered, for example in the Triassic Yanchang Formation of the Erdos Basin,
64 Permian Lucaogou Formation of the Junggar Basin, and the Qingshankou Formation
65 of the Songliao Basin. There are also many important discoveries in the lime-shale of
66 Bohai Bay area and in the Sichuan Basin.^{15,16} Compared with marine shale oil in the

67 North America, the lacustrine shale oil in China is heavier and has higher amounts of
68 polar components; resin and asphaltene is much more abundant than in the North
69 America reservoirs. The presence of these components in the lacustrine shale oil is
70 thought to result in stronger adsorption of oil within the pores of the shale system, which
71 requires extra effort to remove and makes the reservoir more difficult to develop. These
72 polar components should be accounted for in the assessment of shale oil production in
73 China, as they strongly interact with kerogen, minerals, and the widespread nanopores
74 in the shale rock,¹⁷⁻¹⁹ leading to errors in recoverable resource estimation.

75 The adsorption of alkanes on carbonaceous materials, akin to the kerogen, has been
76 studied in recent years. McGonigal et al. directly imaged a two-dimensional, high-
77 degree ordering of the alkane layer at the liquid/graphite interface using a scanning
78 tunneling microscope (STM).²⁰ Castro et al. reported that longer alkanes show a strong
79 preference for adsorption onto graphite.²¹ Furthermore, Severson and Snurr studied the
80 adsorption isotherms of linear alkanes (ethane, pentane, decane, and pentadecane) on
81 activated carbon and evaluated the functions of pore size, chain length, and temperature
82 on adsorption.²² Recently, Harrison et al. studied the single component preferential
83 adsorption of linear and branched alkanes in pores with different apertures (1, 2, and 4
84 nm) at 390 K.²³

85 A similar issue of accounting for hydrocarbons trapped in narrow pores for shale
86 gas has been discussed by Ambrose et al., who suggested that an adjustment of
87 adsorption phase volume is necessary for gas-in-place (GIP) calculations, leading to a
88 10 to 25% decrease in GIP in comparison with the conventional method for
89 assessment.²⁴⁻²⁶ In addition, Wang reported that the unrecoverable fraction of oil-in-
90 place (OIP) is 13% in Bakken shale,²⁷ when taking the adsorption of alkanes in a

91 graphite model into consideration. Nevertheless, there are relatively few studies that
92 explore the effect of polar component adsorption on the estimation of shale oil-in-place.

93 While the interaction of hydrocarbon molecules with pores and surfaces coated with
94 kerogen like materials has been more extensively studied, conceptually shale consists
95 of two parts: organic matter (kerogen) and inorganic matter (minerals). The inorganic
96 part of shale mainly contains quartz, calcite, feldspar and clay minerals. Each kind of
97 mineral makes up a certain volume fraction of a lacustrine/marine shale and plays an
98 important role in shale systems through presenting intra- and inter-particle pore
99 networks that may hold hydrocarbons. Studying the interface of inorganic pores with
100 oil is challenging, and computational chemistry simulations offer great potential to
101 examine the properties of mineral interfaces and oil mixtures at an atomistic level.
102 Previous simulation studies of mineral-organic interfaces have been widespread and
103 extensively studied in the past, such as quartz,²⁸⁻³⁰ calcite,³¹ montmorillonite,³²
104 kaolinite,³³ and muscovite.³⁴

105 Kaolinite often forms surface coatings in the inorganic pores of shale reservoirs, as
106 well as forming pore filling aggregates and presents inter-particle and intra-particle
107 pore surfaces. Kaolinite is different from certain other clay minerals such as illite,
108 smectite, and chlorite due to the octahedral-tetrahedral structure presenting two
109 different surfaces, the mainly oil-wetting silicate surface and the water-wetting
110 aluminol surface. A significant number of computational studies have been published
111 on kaolinite surfaces,^{33,35-44} but these have primarily focused on the adsorption
112 mechanisms of either a single molecule, or a relatively small number of organic
113 molecules to the mineral. As shale oil contains different types and molecular weight
114 alkanes, aromatic hydrocarbons and polar compounds, it is important to study the

115 adsorption of different alkanes in the presence of aromatic and polar compounds to
116 build up a more complete picture of the mineral-oil interface. In addition, temperature
117 and pressure change with depth and maturity in a shale reservoir, therefore it is also
118 important to take these into consideration when considering shale oil adsorption.

119 In this present study, the adsorption behavior of a simple 6-component model crude
120 oil mixture on kaolinite basal surfaces (to represent a shale component) was studied
121 under reservoir conditions using molecular dynamics (MD) simulations. The main
122 objectives were: (1) to provide nanoscale molecular-level resolution for studying the
123 interactions at the hydrocarbon-shale interface; (2) to accurately characterize the
124 adsorption properties of alkanes/polar compounds in the mineral slit-shaped pore space
125 under different temperatures and pressures; (3) to provide improved parameters for the
126 calculation of the unrecoverable fraction for shale OIP (oil-in-place) estimation.

127 **2. MODELS AND SIMULATION DETAILS**

128 The kaolinite unit cell has the chemical formula $\text{Al}_2\text{Si}_2\text{O}_5(\text{OH})_4$, without isomorphic
129 substitutions. The initial atomic positions were taken from the AMCSD (American
130 Mineralogist Crystal Structure Database).^{45,46} This was converted to a cubic cell. The
131 model contained three periodically replicated sheets of kaolinite, creating a clay slab of
132 252 unit cells ($12 \times 7 \times 3$) as shown in Figure 1g, with dimensions of approximately
133 $6.2 \times 6.3 \times 1.9$ nm. The kaolinite structures initially occupied the region $0 < z < 1.9$ nm in
134 all models, and the clay mineral position varied slightly over all timescales modelled.
135 Curtis et al. reported that a large number of nanoscale pores appeared when R_o
136 (reflectance of vitrinite, this reflects the maturity of the shale) is higher than 0.9%.⁴⁷
137 Pores having a size under 20 nm play an important role in the shale systems,⁴⁸ and the

138 8 nm slit-shaped pore (or gallery) in the present model was built to represent these
139 pores.

140 A mixture of methane (CH₄), *n*-hexane (C₆H₁₄), *n*-dodecane (C₁₂H₂₆), *n*-octadecane
141 (C₁₈H₃₈), naphthalene (C₁₀H₈), octadecanoic acid (C₁₈H₃₆O₂) represented the oil
142 mixture molecules in these simulations, (Figure 1a-f). The possible adsorption
143 mechanisms of fatty acids on aluminol surface have been previously studied in the
144 literature, which are mainly caused by hydrogen bonding and Van der Waals interaction
145 in the anhydrous condition.⁴⁹ While classical molecular dynamics (MD) simulation is
146 a powerful technique for understanding the interface structure and dynamics on models
147 of sufficient size to obtain a reasonable degree of complexity, owing to the electronic
148 structure not being included, it cannot be used to predict reactivity. Studies have
149 previously been undertaken looking at reactions of fatty acids at clay mineral interfaces
150 using electronic structure calculations, but on far smaller and less complex model
151 systems.⁵⁰ Classical MD can be used to simulate the formation of pre-reactions
152 configurations and give an indicator of potential reactivity, however this was not
153 undertaken for the present work.⁵¹

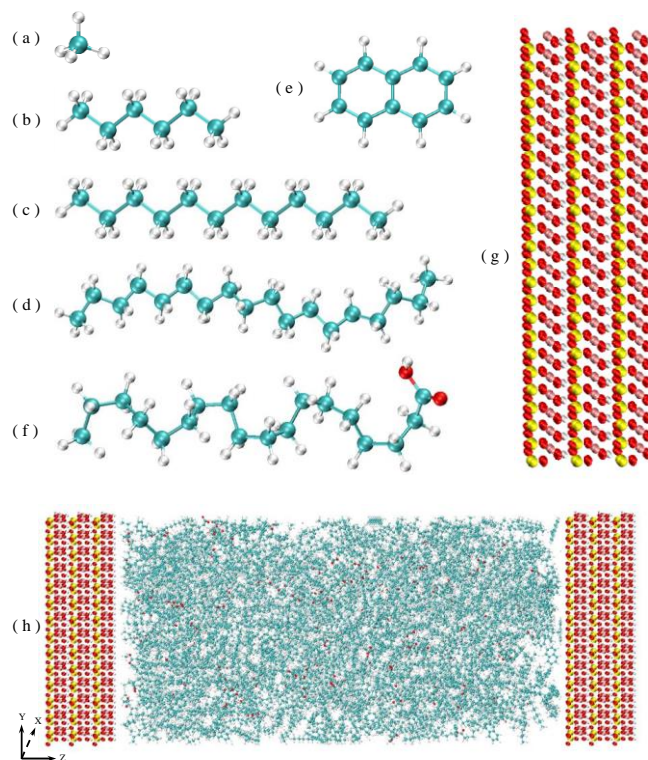
154 In order to compare the adsorption characteristics of multiple components, one
155 hundred and fifty organic molecules were loaded for each component in the models,
156 with the initial percentage of each component at 16.67% by number. Methane
157 molecules were used to represent gas dissolved in the shale oil (C₁-C₅ fraction), *n*-
158 hexane and *n*-dodecane molecules for the low carbon number alkanes (C₆-C₁₄ saturated
159 hydrocarbon), *n*-octadecane molecules for high carbon number alkanes (C₁₅₊ saturated
160 hydrocarbon), naphthalene molecules for aromatic hydrocarbons (C₆₊ aromatic
161 hydrocarbon) and octadecanoic acid molecules for polar compounds (resin and

162 asphaltene). The adsorbed molecules were inserted using the program PackMol,⁵²
163 resulting in the system presented in Figure 1h.

164 The ClayFF force field and the CHARMM36/CGenFF force field were used to
165 model the kaolinite clay mineral basal surfaces, and the organic oil molecules
166 respectively within the simulations.⁵³⁻⁵⁶ Both of these two force fields have recently
167 been tested in conjunction, and the interacting properties between hydrated mineral
168 surfaces and organic molecules can be accurately reproduced using ClayFF and
169 CHARMM36/CGenFF force field.⁵⁷ Previous simulations have shown that the
170 adsorption of organic molecules (which were parameterized with CHARMM/CGenFF)
171 on quartz surfaces (which were parameterized with ClayFF) are not only consistent
172 with *ab-initio* molecular dynamics, but also with experimental X-ray reflectivity data.⁵⁸
173 Intermolecular organic-clay mineral interactions were modelled using Lorentz-
174 Berthelot mixing rules.

175 All simulations were performed using the MD suite, GROMACS 4.6.7.^{59, 60} Real-
176 space particle-mesh-Ewald (PME) electrostatics and a van der Waals cutoff of 1.4 nm
177 were used in all simulations. The parameters used in energy minimization and
178 equilibration period were the same as Underwood et al.³³ This equilibration simulation
179 was followed by a 200 ns production run in the NPT ensemble using a velocity-rescale
180 thermostat, with a temperature coupling constant of 1 ps, and a semi-isotropic
181 Parrinello-Rahman barostat, with a pressure coupling constant of 1 ps. The simulations
182 were run under several conditions: 1) a pressure of 100 bar and a temperature of 323
183 K, which represents the geological conditions of the Nenjiang Formation in Songliao
184 Basin,⁶¹ and 2) three more temperature points (298 K, 348 K and 373 K at 100 bar) and
185 three more pressure points (1 bar, 50 bar and 200 bar at 348 K) were set in order to

186 study the influence of temperature and pressure on the oil adsorption, for the
187 temperatures and pressures reflect the main distribution of the oil-window stage in the
188 Nenjiang Formation.



189

190 Figure 1. The molecules in the oil mixture: (a) methane (CH_4), (b) *n*-hexane (C_6H_{14}), (c) *n*-dodecane
191 ($\text{C}_{12}\text{H}_{26}$), (d) *n*-octadecane ($\text{C}_{18}\text{H}_{38}$), (e) naphthalene (C_{10}H_8), (f) octadecanoic acid ($\text{C}_{18}\text{H}_{36}\text{O}_2$), (g)
192 kaolinite surfaces, and (h) starting configuration of oil mixture in the kaolinite nanopore.

193 All simulation trajectories have been captured using VMD 1.9.2.⁶² The color
194 scheme of all snapshots is defined as follows. The clay structure contains silicon
195 (yellow), oxygen (red), aluminum (pink), and hydrogen (white) atoms. Organic
196 molecules contain carbon (cyan), hydrogen (white) and oxygen (red). The
197 atomic/molecular densities of the oil mixture across the nanopore were calculated using
198 the analysis tools within GROMACS 4.6.7, and subsequently plotted using Matlab
199 2017. Owing to some of the simulations only reaching equilibrium at 140 ns (see
200 determination of equilibrium in ESI), in order to increase the statistics of the

201 simulations, the simulation time was extended to 200 ns, and the last 60 ns was selected
202 to calculate the density profiles and undertake analysis of oil partitioning. Full details
203 of the analysis of the model oil partitioning are given in the ESI.

204 **3. RESULTS AND DISCUSSION**

205 **3.1 Volume and density of adsorption of oil phase molecules.**

206 To gain insight into the adsorption behavior of the six-component oil mixture molecules
207 confined in the kaolinite nanopore, which consists of opposing silicate and aluminol
208 surfaces, local density distributions and configurations of different components after
209 equilibration were collected for oil mixtures within a 7.82 nm interlayer (representing
210 the nanopore space between the kaolinite sheets) at 323 K, 100 bar (Figure 2). The
211 continuous mass density profile (collected by partitioning the simulation box into layers
212 of 0.015 nm) normal to the kaolinite surface was calculated using the final 60 ns of
213 simulation data and the last frame of the production model was captured as a snapshot
214 to show the oil mixture distribution in region between the kaolinite sheets (Figure 2a).
215 Figure 2b shows that the oil mixture molecules are not uniformly distributed throughout
216 the slit-shaped pore, and the density is not symmetrical about the center line of the two
217 interfaces. Owing to the strong intermolecular affinities between the kaolinite mineral
218 sheets and the alkanes, increased order of the oil components through layering is
219 evident in the mass density near the mineral interface, and the magnitude of the ordered
220 arrangement gradually reduces with increasing distance from the aluminol and silicate
221 surfaces, which varies depending on the nature of the molecule. In the bulk region, the
222 computed mass density remains almost constant. The first density peak adjacent to the
223 aluminol surface is 1887 kg/m^3 , which is approximately 1.5 times greater than that of

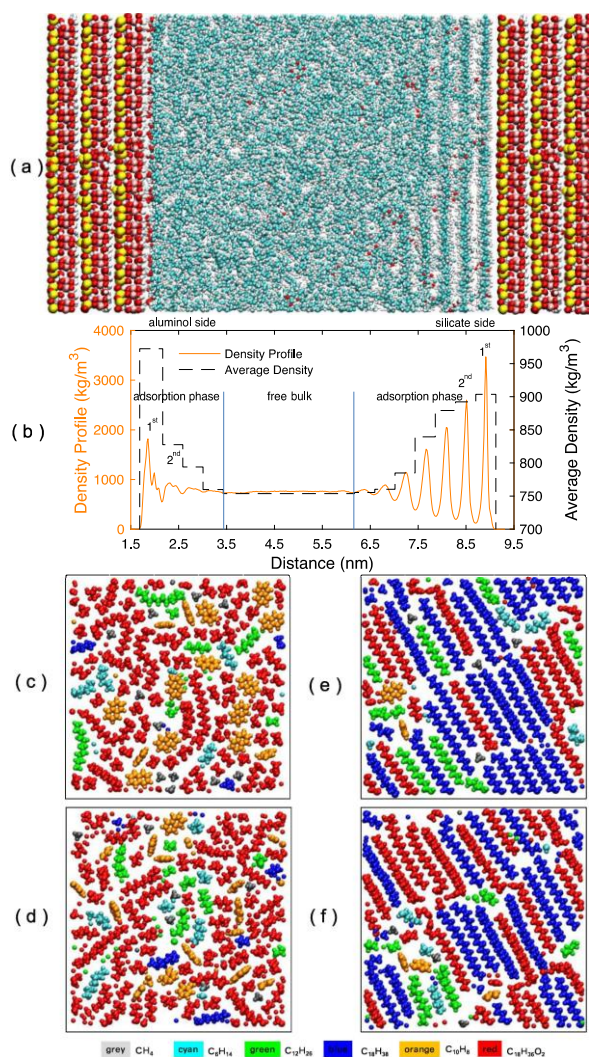
224 the bulk fluid (764 kg/m^3); on the opposite side, the first density peak adjacent to the
225 silicate surface is 3404 kg/m^3 , which is approximately 3.5 times greater than that of the
226 bulk fluid. Such high density is due to the increased order in the close packed 2-
227 dimension layers, making it into a relatively immobile solid-like state.^{27,63} Away from
228 the kaolinite interface region, surface induced structuring contributes a diminishing
229 influence on the mass density, thus leading to a lower density peak of 999 kg/m^3 on the
230 aluminol surface and 2519 kg/m^3 on the silicate surface. In the slit-shaped pore mid-
231 plane, the physical properties of the bulk fluid show no strong fluctuations.

232 With the objective of determining an improved estimate of the recoverable oil-in-
233 place, the volume occupied by the adsorption phase, which exists in a solid-like state,
234 must be determined and deducted from the total pore space. The mass density profiles
235 of the oil mixture in the kaolinite model (Figure 2a and 2b) reveal the adsorption region,
236 defined as the region in which their local density deviates from the bulk value.⁶⁴⁻⁶⁶
237 Recent studies of liquid structure theory modelling for non-attractive hard spheres also
238 show pronounced oscillations in the density close to a boundary surface, with
239 Davidchack et al. showing these oscillations are caused by the surface providing a
240 translational plane, rather than the molecules adhering to the surface.⁶⁷ Although
241 density oscillations are found in liquid structure models with no attractive potential
242 between the surface and the molecules, the average density of the “oscillation” region
243 at the boundary is almost the same as that in the bulk region. The average density of
244 each adsorption layer was also calculated for the kaolinite pore and analyzed (eq S1).
245 The result shows that average density of oil mixture in the adsorption region is
246 significantly greater than that in the bulk region (Figure 2b), evidencing adsorption on
247 the surface. The oil mixture contains four adsorption layers on the aluminol surface and

248 seven on the silicate surface, indicating differential multi-layer adsorption of oil
249 mixture molecules on the surface of kaolinite sheets. The solvation forces between *n*-
250 alkanes and mica surfaces, measured by Christenson et al.,⁶⁸ showed decaying layered
251 structuring, and the interlayer spacing observed (0.40-0.50 nm) was approximately
252 equal to the width of alkane molecules, while independent of the chain length (1.35 nm
253 for *n*-octane). Our analysis shows that the layer thickness is ~0.44 nm on the aluminol
254 surface and ~0.42 nm on the silicate surface (Figure 2b), in good agreement with the
255 above experimental results. Figure 2b also shows that the fluctuation of mass density
256 extends 1.77 nm and 2.96 nm for the aluminol surface and silicate surfaces,
257 respectively, suggesting that, under these conditions, and for a 7.82 nm pore with
258 kaolinite surfaces, the adsorbed hydrocarbon phase accounts for 60.4% of the pore
259 volume. The adsorption phase mass transfer ratio (eq S2) in the 8 nm kaolinite mineral
260 pore is 65.7 % in the kaolinite pore. The C_{ada-a} and C_{ads-a} of the aluminol and silicate
261 surfaces are, respectively, 1.44 mg/m² and 2.47 mg/m² (Through eq S3 and eq S4). For
262 the model oil studied, the adsorption capacity of the silicate surface is much greater
263 than that of the aluminol surface.

264 Additionally, in order to investigate the oil mixture adsorption characteristics on
265 kaolinite surfaces, in-plane cross-section images are taken to show the first and second
266 adsorption layer on both the aluminol and silicate surfaces (Figure 2c-f). In the first
267 adsorption layer on the aluminol mineral interface, octadecanoic acid and naphthalene
268 occupy most of the surface area and are distributed with no apparent order (Figure 2c),
269 as in the second adsorption layer (Figure 2d). When compared to the aluminol surface,
270 on the silicate surface the octadecanoic acid and *n*-octadecane distribute in an ordered
271 manner, with a 30° angle between the *n*-octadecane molecules long axis and the

272 crystallographic y direction, shown as a blue dashed line in Figure 2e, which is
273 determined by the crystal lattice symmetry. As a comparison, Dirand, et al. found that
274 the distance between n -octadecane molecules between planes in the crystal structure of
275 n -octadecane is 0.48 nm,⁶⁹ which is 0.03 nm larger than that observed here on the
276 silicate surface. This indicates that n -octadecane molecules arrange closer due to the
277 hexagonal lattice of the silicate side. However, the thickness in the crystallographic z
278 direction is 0.40 nm, which is 0.04 nm smaller than that on the silicate surface. That is
279 because the temperature in this simulation is 323 K, which is 30 K higher than the n -
280 octadecane crystallization temperature. Even though the n -octadecane molecules are
281 attracted towards the silicate surface, temperature plays an important role in the
282 adsorption characteristics. The n -octadecane molecules formed in a more crystal-like
283 state, but still containing molecular gauche conformers and torsion of the chains of
284 alkanes. As such, the thickness of one adsorption layer is larger than the thickness of a
285 similar layer of crystalline n -octadecane.⁶⁹ Small molecules (methane, n -hexane and
286 naphthalene) are arranged in the interstices formed between the regions occupied by n -
287 octadecane and octadecanoic acid. This suggests some molecular sized nanoporosity is
288 formed by imperfect packing of larger organic molecules on the mineral surface. The
289 model oil molecules in the second adsorption layer on the silicate surface are more
290 disordered than the first adsorption layer, as evidenced by the increased distance
291 between them and the silicate surface (Figure 2f).



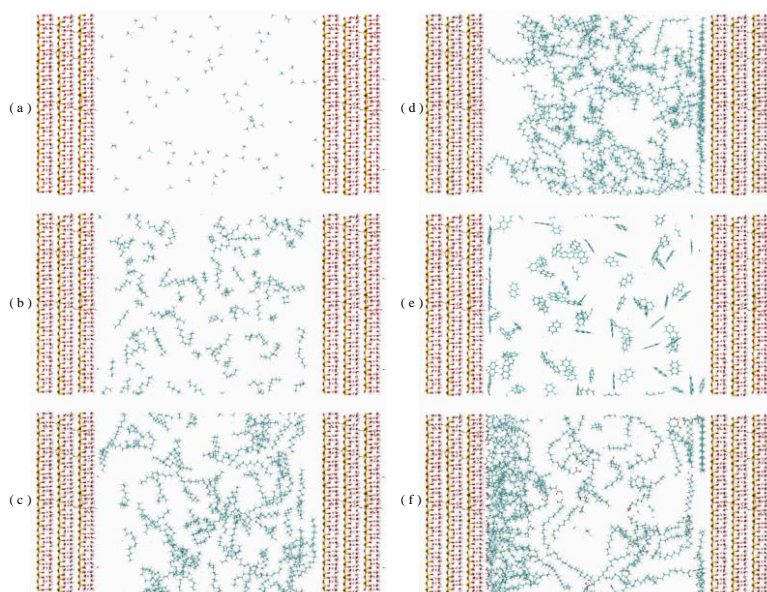
292

293 Figure 2. The adsorption of the 6-component oil mixture in a 7.82 nm kaolinite pore (323 K, 100
 294 bar) showing: (a) Snapshot of the final frame of the simulation; (b) Mass density profiles across the
 295 pore; (c) Cross section snapshot showing the first adsorption layer on the aluminol surface; (d) Cross
 296 section snapshot showing the second adsorption layer on the aluminol surface; (e) Cross section
 297 snapshot showing the first adsorption layer on the silicate surface; (f) Cross section snapshot
 298 showing the second adsorption layer on the silicate surface.

299 3.2 Comparison of the adsorption characteristics of multiple 300 components on both surfaces of kaolinite

301 Here, the adsorption character and mole number density of each component in the six-
 302 component oil mixture on kaolinite surfaces are discussed. Firstly, a snapshot of the last
 303 frame of oil mixture adsorption simulation is taken to show the qualitative evaluation
 304 of each component adsorption character of the oil mixture in the kaolinite model

305 (Figure 3). Each component is displayed separately on Figure 3a to Figure 3f. We can
306 see from Figure 3a that methane is mainly distributed evenly in the kaolinite slit-shaped
307 pore. Figure 3b shows that *n*-hexane has little affinity for either surface of the kaolinite,
308 but is still evenly distributed throughout the slit-shaped pore. However, the long
309 alkanes, *n*-dodecane and *n*-octadecane, are more likely to be adsorbed on the silicate
310 surface (Figure 3c and 3d). The majority of the *n*-octadecane are observed on the silicate
311 surface in the first adsorption layer. In contrast, naphthalene and octadecanoic acid have
312 a higher probability of being adsorbed on the aluminol surface. This is due to the
313 attractive forces between the conjugated π -system of naphthalene and the slightly
314 positively charged hydrogen atoms of the kaolinite aluminol surface, as well as the
315 polar interactions and hydrogen bonding between the carboxylate groups and the
316 hydroxyl groups for octadecanoic acid (Figure 3e and 3f).



317

318 Figure 3. Snapshot showing the adsorption characteristics of each of the six oil components in a
319 7.82 nm kaolinite slit-shaped pore at 323 K and 100 bar: (a) methane; (b) *n*-hexane; (c) *n*-dodecane;
320 (d) *n*-octadecane; (e) naphthalene; (f) octadecanoic acid

321 Mole number density profiles of each component in the oil mixture were
322 calculated to evaluate the adsorption characteristics quantitatively using eq S9 (Figure

323 4a and 4b). The mole number density profile of methane shows four distinct adsorption
324 layers on the aluminol surface, and the first adsorption layer peak value is a little higher
325 than that of bulk (Figure 4a). The thickness of each monolayer is 0.42 nm, by which
326 the mole number density profile is determined. In contrast to the aluminol surface, the
327 mole number density profile of methane on the silicate surface shows seven distinct
328 adsorption layers, but most are lower than the pore center region (Figure 4b). This
329 phenomenon is not like the single component methane adsorption characteristics on the
330 Na-montmorillonite surface, which has only one major adsorption layer where the
331 density value is almost 4 times greater than that of bulk methane,⁷⁰ owing to the
332 existence of the other oil components. The methane molecules are not only adsorbed
333 on the mineral surface, but also become dissolved in the oil mixture.

334 The adsorption mole number density profiles of liquid hydrocarbons (*n*-hexane, *n*-
335 dodecane, *n*-octadecane) on the aluminol surface show that there are also four
336 adsorption layers (Figure 4a), as for methane. Also, the density values of the adsorption
337 layers are lower than in the bulk (slit-shaped pore middle) region, indicating that the
338 liquid hydrocarbons are less likely to adsorb on the aluminol surface. In contrast, there
339 are seven adsorption layers of liquid hydrocarbons on the silicate surface and the
340 density values are much higher than in the bulk region. This is especially the case for
341 the longer *n*-octadecane molecules, which occupy almost half of the first adsorption
342 layer's available surface area at the interface. Within the first four adsorption layers on
343 the silicate surface, which is the region most influenced by the kaolinite sheet, the
344 values of the mole number density profiles peaks were found to decrease with the
345 alkane chain length ($\rho_{\text{mol-C}_6\text{H}_{14}} < \rho_{\text{mol-C}_{12}\text{H}_{26}} < \rho_{\text{mol-C}_{18}\text{H}_{38}}$), as shown in Figure 4b.

346 The aromatic hydrocarbon (naphthalene), mainly adsorbs directly onto the

347 aluminol surface, and not on the silicate surface, as indicated by a single prominent near
348 surface peak in the density profile at the aluminol interface (Figure 4a), with a value of
349 6.20 kmol/m^3 which is over 6 times greater than the bulk density (0.87 kmol/m^3).
350 Although there are seven adsorption layers on the silicate surface, the density values of
351 each are much lower than that of the bulk (Figure 4b), which is in accord with the
352 snapshot showing the adsorption characteristics of the individual component in Figure
353 3e. This indicates the naphthalene adsorption capacity on, and interactions with, the
354 aluminol surface are much higher than on the silicate surface.

355 The density profile for the adsorption of the polar octadecanoic acid (Figure 4a
356 and 4b) showed three adsorption layers on the aluminol surface and six layers on the
357 silicate surface. The density of octadecanoic acid in the bulk region is the lowest,
358 indicating octadecanoic acid is likely to be adsorbed the most, compared with the other
359 oil components. There are two distinct peaks in the octadecanoic acid density in the
360 first adsorption layer on the aluminol surface, which is different from the other oil
361 components. The head group (carboxylate group) of the octadecanoic acid molecule is
362 adsorbed on the aluminol surface, with hydrogen bonding to the Al-OH groups partly
363 suggested by the visual analysis, as can be observed in in Figure 3f. This results in the
364 hydrophobic alkyl chain orienting away from the surface. This can be contrasted with
365 the silicate interface, where the alkyl chain can be observed bonded on and parallel to
366 the kaolinite mineral surface, with the carboxylate head group oriented away from the
367 surface. These results are consistent with the work of Underwood et al.³³ On the silicate
368 surface, the octadecanoic acid molecules are adsorbed with an almost parallel
369 orientation to the silicate surface, with a gauche conformation, similar to the *n*-
370 octadecane molecules. The octadecanoic acid forms only one peak in the first

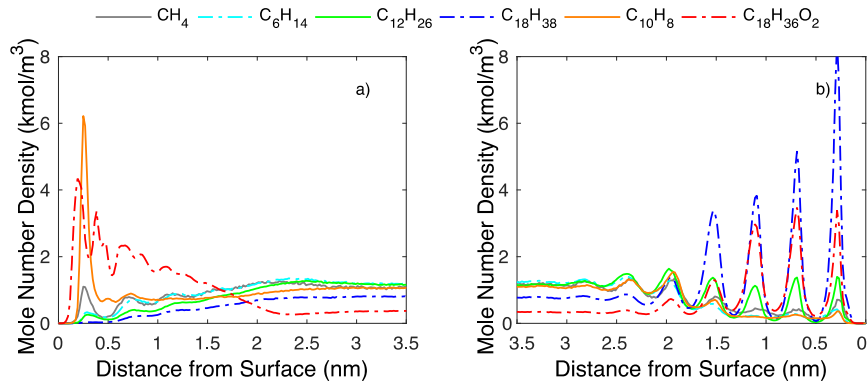
371 adsorption layer, with five density peaks having values higher than that of the mid-
372 plane (bulk) region and the density of the first layer is not higher than that of the second
373 layer, owing to the competitive adsorption of *n*-octadecane.

374 Additionally, in order to compare the adsorption characteristics of the six
375 components, the adsorption percentage of each individual component in the different
376 adsorption layers was calculated (eq S10). Mole number percentage of six components
377 on the aluminol side shows that naphthalene and octadecanoic acid occupy almost 85
378 % of first adsorption layer (Figure 5a). Both of these molecules follow the trend that
379 adsorption percentage decreases with the number of adsorption layers (this
380 phenomenon can be called a positive adsorption trend). However, the alkanes have a
381 contrary trend (this phenomenon can be called a negative adsorption trend), furthermore
382 the adsorption percentage of each component in the four adsorption layers decreases as
383 the carbon number increases.

384 On the silicate surface, *n*-octadecane has a trend that adsorption percentages
385 decrease with the number of adsorption layers, which is different from the trend on the
386 aluminol surface, indicating *n*-octadecane is more likely to be adsorbed on the silicate
387 surface (Figure 5b). Adsorption percentages of methane, *n*-hexane, *n*-dodecane increase
388 with the number of adsorption layers, the same trend as on the aluminol surface,
389 indicating they are less likely to be adsorbed on both surfaces of kaolinite compared
390 with the other three components. Naphthalene also has a negative adsorption trend on
391 the silicate surfaces, similar to methane, *n*-hexane, and *n*-dodecane, which is different
392 from the trend on the aluminol surface, and it indicates that naphthalene is likely to be
393 adsorbed preferentially on aluminol surfaces. Meanwhile, the adsorption percentage of
394 each liquid alkane component (*n*-hexane, *n*-dodecane, *n*-octadecane) in the first four

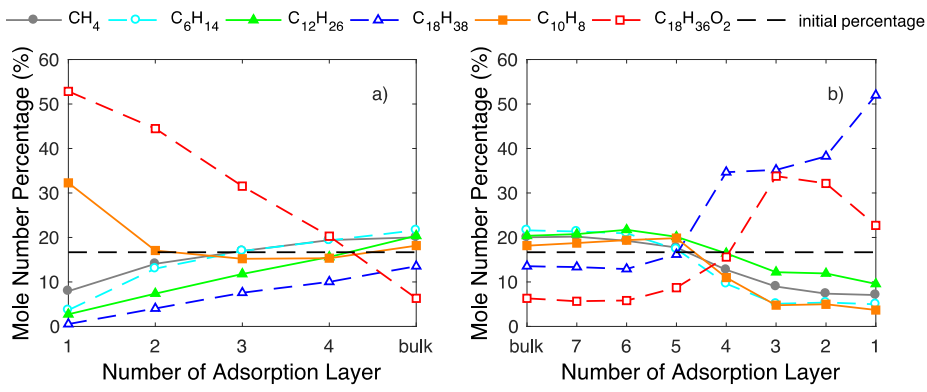
395 adsorption layers increases with increasing number of carbon atoms in the chain.

396 After comparing the adsorption character and mole number density profile of the
397 six components in the oil mixture on kaolinite surfaces, it can be concluded: 1) the
398 number of adsorption layers, density of each adsorption layer and total adsorption
399 capability on the aluminol surface are all smaller than those on the silicate surface; 2)
400 the surface lattice structure of the silicate surface guides the arrangement of oil
401 molecules, whereas the aluminol surface does not; 3) aromatic naphthalene and polar
402 octadecanoic acid molecules are more likely adsorbed on the aluminol surface, while
403 *n*-octadecane molecules are more likely to be found adsorbed on the silicate surface.
404 Meanwhile, the percentage of alkane molecules in the adsorption layers on the silicate
405 surface increases as the number of carbon atoms increases; 4) alkanes have a negative
406 adsorption trend on aluminol surfaces, and naphthalene and octadecanoic acid have a
407 positive adsorption trend; 5) the *n*-octadecane molecules have a positive adsorption
408 trend, meanwhile methane, *n*-hexane, *n*-dodecane and naphthalene have a negative
409 adsorption trend on the silicate surface. This partitioning is important as oil mixture
410 components' adsorption characteristics play an important role in determining the
411 surface tension and nano-scale flow mechanism of the oil in the pores. Additionally,
412 this principle can also be applied to light hydrocarbon recovery in shale oil recovery
413 evaluation and enhanced oil recovery more generally.



414

415 Figure 4. Analysis of the mole number density profiles of the six oil components on: (a) the
416 aluminol surface; (b) the silicate surface.



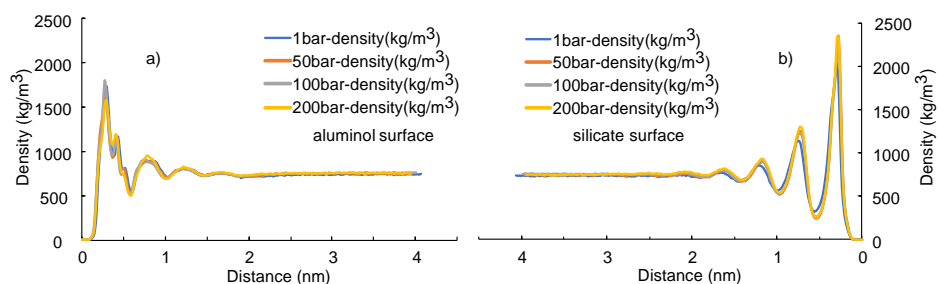
417

418 Figure 5. Mole number percentage of the six oil components on (a) the aluminol surface. (b) the
419 silicate surface.

420 3.3 Effect of pressure on oil mixture adsorption.

421 In this section, we discuss the influence of pressure on the adsorption characteristics of
422 the multiple oil components. Mass density profiles of the oil mixture at four different
423 pressure points (1 bar, 50 bar, 100 bar, 200 bar) are imaged on both sides of the kaolinite
424 slit-shaped pore (Figure 6a and 6b). Firstly, the thickness of the adsorption layer extends
425 very slightly with the increase of pressure. Meanwhile, as the pressure rises, the number
426 of adsorption layers remains the same on both surfaces of the kaolinite sheets (four
427 layers on the aluminol surface and five layers on the silicate surface). In addition, the
428 density of the oil mixture has small changes with pressure and the thickness of

429 adsorption layers decreases slightly with pressure on silicate surfaces. This is because
430 as the pressure increases, the force exerted on the system increases and this will lead to
431 closer packing of the oil molecules. Therefore, the density peak has a slight increase,
432 commensurate with a decrease in the thickness of the initial layer, though, overall,
433 pressure appears to have only a small effect.



434

435 Figure 6. Mass density profiles for oil mixture at different pressures on kaolinite surface: (a) the
436 aluminol surface; (b) the silicate surface.

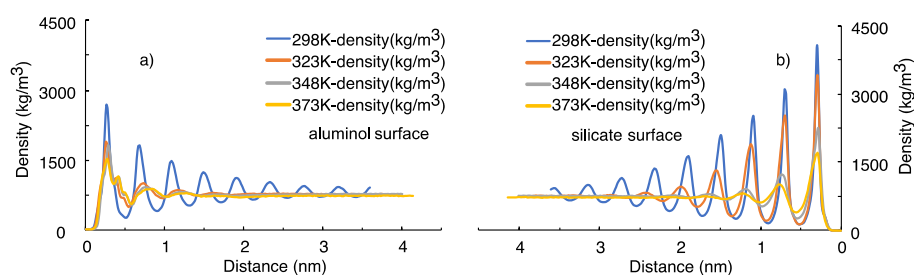
437 **3.4 Effect of temperature on 6-component oil mixture adsorption.**

438 In this section, the influence of temperature on the adsorption characteristics of the six
439 components of the oil mixture is studied. The mass densities at four different
440 temperatures (298 K, 323 K, 348 K and 373 K) were plotted for both basal surfaces of
441 the kaolinite model (shown in Figure 7a and 7b). The mass density profiles start from
442 the surface of the kaolinite sheets and end in the mid-point of the oil mixture where
443 more bulk like behavior is expected. Firstly, we can see that the lengths of the profiles
444 extend with the increase of temperature, i.e. the bulk density of the oil mixture decrease
445 with increased temperature. It can also be noted that, as the temperature rises, the
446 number of adsorption layers on the aluminol surface drops from six to three (six layers
447 at 298 K, 4 at 323 K, four at 348 K and three at 373 K), and on the silicate surface it
448 drops from seven to five (seven layers at 298 K and 323 K, five at 348 K and 373 K).
449 Although the thickness of each adsorption layer increases with temperature, the mass

450 density, the total thickness of the adsorbed layer and the total adsorption capability have
451 different trends on the opposing sides of the kaolinite pore, with the silicate and
452 aluminol layers showing distinct behaviors. It is notable that each mass density peak
453 maxima of the adsorption layers moves further from the surface of the kaolinite with
454 increased temperature (the position of second density peak maxima on the silicate
455 surface: 0.69 nm at 298 K; 0.69 nm at 323 K; 0.74 nm at 348 K; 0.78 nm at 373 K),
456 with the exception of the first adsorption layer peak maxima (the position of first
457 density peak maxima on the silicate surface is almost 0.29 nm at all four temperature
458 points), where the change is negligible. This indicates that, independent of the
459 temperature, the arrangements of the oil mixture components and the mass center of the
460 first adsorption layer are almost the same, with small changes caused by the gauche
461 conformers and torsion of the chains of alkanes and octadecanoic acid. It can also be
462 noticed that there is only single peak maxima in the first adsorption layer on the
463 aluminol surface at 323 K, which is different from the other three temperatures studied.
464 This arises due to the arrangement of octadecanoic acid molecules on the aluminol
465 surface at 323 K being the same as that on the silicate surface, where the molecules are
466 adsorbed with in an almost parallel orientation to the aluminol surface, with a zigzag
467 arrangement.

468 It is useful to compare the thickness of each adsorption layer on the silicate
469 surface, at the four temperatures, with the inter-molecular plane packing thickness of
470 *n*-octadecane in a crystalline state (293 K), which was measured by Dirand, et al.⁶⁹ The
471 thickness of each adsorption layer at the four temperatures is 0.41 nm, 0.42 nm, 0.43
472 nm and 0.44 nm in the *z* direction for 298 K, 323 K, 348 K and 373 K, respectively.
473 These are comparable to the 0.40 nm distances experimentally reported in crystalline

474 *n*-octadecane at 293 K. The slight (under 10%) increase of these values arises from: 1)
 475 with the increase of temperature gauche conformations in the alkane chain are more
 476 common, as well as appearance of rotatory states due to thermal motion of the
 477 molecules; 2) the oil mixture in this simulation contains several small molecules (such
 478 as methane, *n*-hexane) dissolved in the longer chain molecules, which will lead to the
 479 increase of the adsorption layer thickness.



480

481 Figure 7. Mass density profiles for oil mixture at different temperatures on the kaolinite surface: (a)
 482 the aluminol surface; (b) the silicate surface.

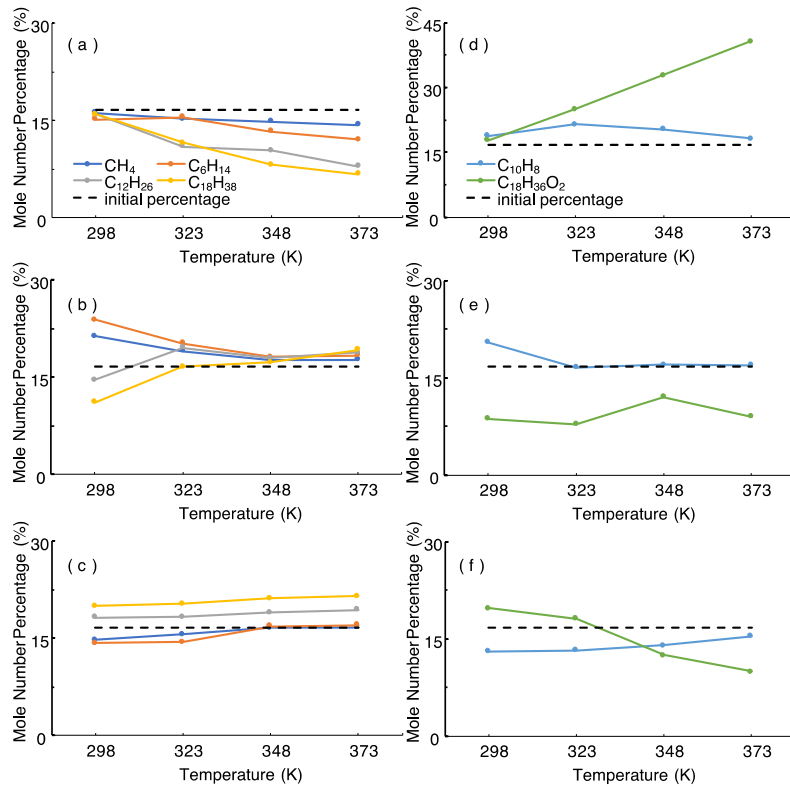
483 Additionally, in order to compare the adsorption characteristics of the six
 484 components at four temperatures quantitatively, the adsorption percentages of
 485 individual component in a defined adsorption region on both sides of the kaolinite
 486 sheets was calculated through eq S11. Plot figures of the mole number percentage of
 487 the six components on the aluminol interface show that naphthalene and octadecanoic
 488 acid occupy almost 85% of space in the first adsorption layer. Figure 8a-c shows the
 489 mole number percentage of alkanes (methane, *n*-hexane, *n*-dodecane and *n*-octadecane)
 490 at the four different temperatures on the aluminol surface, the bulk region and on the
 491 silicate surface, respectively. Figure 8e-f show the same data for naphthalene and
 492 octadecanoic acid, at four different temperatures on the aluminol surface, in the bulk
 493 region and on the silicate surface, respectively. The black dashed line shows the initial
 494 percentage of each component in the kaolinite model (i.e. 16.67 %). The mole number

495 percentage of alkanes in the adsorption region on the aluminol surface decrease with
496 the rise in temperature, and they are all lower than the initial percentage, which
497 indicates that alkanes are not likely to be adsorbed on the aluminol surface. At lower
498 temperature (298 K) the percentages of alkanes are almost the same as one another,
499 and, as such, very near to the initial percentage, however, with the increase of
500 temperature, the percentages of alkanes with a high carbon number in the interfacial
501 region decrease faster than those alkanes with a low carbon number. At 373 K, the
502 percentages of the alkanes are separated by the largest amount relative to each other.
503 The order of percentages of alkanes on the aluminol surface is methane<*n*-hexane<*n*-
504 dodecane<*n*-octadecane, which are 14.4%, 12.1%, 7.9% and 6.8%, respectively (Figure
505 8a). When the percentage of octadecanoic acid on the aluminol side is considered, it
506 has a regular linear growth trend with the increase in temperature. However, the
507 naphthalene has a slightly decreasing trend. Furthermore, the percentages of both the
508 octadecanoic acid and naphthalene are higher than the initial (16.6%) percentage, which
509 indicate that they are more likely to be adsorbed on the aluminol surface than the
510 alkanes (Figure 8d) and octadecanoic acid has the biggest percentage in the adsorption
511 region on the aluminol side.

512 In this section, we discuss the adsorption percentage of six components on the
513 silicate surface. Here, the alkanes have an opposite trend to that observed above on the
514 aluminol surface, with increasing adsorption percentages as temperature increases.
515 Alkanes with a high carbon number are adsorbed preferentially on the silicate surface
516 than alkanes with a lower carbon number, which is again a different trend to that
517 observed on the aluminol surface (Figure 8c). For the percentages of octadecanoic acid
518 and naphthalene on the silicate side, octadecanoic acid decreases with increasing

519 temperature. Naphthalene shows a slight increase in adsorption with temperature
520 increase. Meanwhile, both molecules show relatively lower adsorbed amounts than the
521 initial percentage, which indicates that they are less likely to be adsorbed on the silicate
522 surface, especially at higher temperatures (Figure 8f).

523 Finally, we analyze the percentage of multiple components in the bulk region,
524 which also reflects the percentage of total adsorption capacity on the different basal
525 surfaces of the kaolinite sheets. At 298 K, the percentage of the alkanes with low carbon
526 number (methane and *n*-hexane) are higher in the bulk region than longer alkanes,
527 however, with increased temperature the percentages of alkanes begin to converge,
528 approaching the initial percentage. At 373 K, the order of alkane abundance in the bulk
529 region is methane<*n*-hexane<*n*-dodecane<*n*-octadecane, which are 17.7%, 18.4%,
530 18.8% and 19.2%, respectively (Figure 8b). This indicates that the alkanes with higher
531 carbon number are more likely to be adsorbed on both surfaces of the kaolinite sheets
532 at low temperature and become more mobile and release at high temperature. The
533 change in distribution percentage of naphthalene in the bulk has the same trend as that
534 of the alkanes with low carbon number and it is almost the same as the initial
535 percentage. This indicates that the percentage of naphthalene in the bulk region is the
536 same with that in the near-surface region. Percentage analysis of the octadecanoic acid
537 shows it does not have a definite trend, though as they are all less than the initial
538 percentage this indicates that octadecanoic acid molecules are adsorbed more on the
539 surfaces, overall.



540

541 Figure 8. Mole number percentage of six components at different temperatures in kaolinite sheets
 542 (a) alkanes on aluminol side; (b) alkanes in bulk region; (c) alkanes on silicate side; (d) naphthalene
 543 and octadecanoic acid on aluminol side; (e) naphthalene and octadecanoic acid in bulk region; (f)
 544 naphthalene and octadecanoic acid on silicate side.

545 4. CONCLUSIONS

546 In this work, we perform a study of the adsorption characteristics of a multi-component
 547 oil mixture in a kaolinite nano-scale slit-shaped pore to represent intra-particle pores
 548 within a shale oil system. We discuss the total adsorption phase thickness in the
 549 nanopore and the characteristics of each component. The main conclusions of the study
 550 are:

- 551 (1) Under reservoir conditions (323 K, 100 bar), there are four distinct adsorption layers
 552 of oil components on aluminol surfaces and seven layers on silicate surfaces, and
 553 the thickness of each layer is 0.44 nm on the aluminol surface and 0.42 nm on the
 554 silicate surface. In addition, the adsorption capacity per unit area of aluminol and

555 silicate surface is 1.44 mg/m² and 2.47 mg/m² respectively. The silicate surface
556 orders the arrangement of adsorbed molecules, and the adsorption capacity and
557 density are higher than that of the aluminol surface.

558 (2) Naphthalene and octadecanoic acid are more likely to be adsorbed on the aluminol
559 surface, meanwhile, heavier hydrocarbons (*n*-octadecane) and octadecanoic acid
560 are more likely to be adsorbed on the silicate surface. With the increase of carbon
561 number, the adsorption percentages of the linear alkanes decrease in adsorption
562 layers. In addition, alkanes have a “negative adsorption trend” on aluminol surface,
563 while, naphthalene and octadecanoic acid have a “positive adsorption trend”. In
564 contrast, the trend on silicate surfaces is opposite to that on aluminol surfaces.

565 (3) Pressure has little influence on the adsorption of the oil mixture. With the increase
566 of temperature, the thickness, density of adsorption layer, number of adsorption
567 layers and total adsorption amount decreases on both surfaces of kaolinite sheets.
568 On the aluminol surface, the percentage of polar compounds increase, while the
569 presence of alkanes decreases with temperature. And at higher temperature (348 K
570 and 373 K), the percentage of alkanes decrease with carbon number. However, these
571 trends on the silicate surface are opposite to those found on the aluminol surface.
572 At lower temperatures enthalpy driven interactions are more important than
573 entropic ones. This explains the varying adsorption of oil components on different
574 kaolinite surfaces. At higher temperatures, entropy becomes more relevant, thus
575 leading to reduction in surface selectivity.

576 The findings illustrate that in nano-pores in oil and gas reservoirs, layers of strongly
577 bound oil profoundly modify the available pore volume. Critically, the presence of

578 different mineral surfaces can selectively remove different components of crude oil and
579 this is likely to be particularly important when considering oil migration pathways and,
580 especially, when considering surface wetness modification in enhanced oil recovery.
581 Given the recent increase in resolution in computer tomography and mineral/pore
582 mapping capabilities,⁷¹ this present study allows the properties of identified pores to be
583 further explored. Future work will explore the effect of pH and surface defects on the
584 surface adsorption characteristics of the model oil. Furthermore, the parameters
585 obtained here allow us to explore further recovery models for shale oil systems.

ACKNOWLEDGEMENTS

This study was partly funded by the National Natural Science Foundation of China (41572122, 41330313, 41672116), National Science and Technology Major Project (2016ZX05004-001, 2016ZX05007-003), National Basic Research Program of China (973 Program) (2014-CB239005), Graduate Innovation Fund of China University of Petroleum (YCXJ2016004). The first author also would like to acknowledge the China Scholarship Council (CSC) for its financial support for his living expenses at Durham University, UK as a visiting Ph.D. student. We gratefully acknowledge Prof. H. Chris Greenwell for providing the opportunity for ST to visit the Greenwell research group. HCG thanks the Royal Society for funding via an Industry Fellowship, while HCG and TRU also wish to acknowledge funding from BP.

DECLARATIONS

Conflict of interest: We declare that we have no financial or personal relationships with other people or organizations that can inappropriately influence our work, there is no professional or other personal interest of any nature or kind in any product, service and/or company that could be construed as influencing the position presented in, or the review of, the manuscript entitled, “Understanding model crude oil component interactions on kaolinite silicate and aluminol surfaces: towards improved understanding of shale oil recovery”.

Ethical approval: Not required

AUTHOR CONTRIBUTIONS

Shansi Tian performed the molecular simulations and wrote the main manuscript. Valentina Erastova provided the Gromacs software training, the method for solving problems in the simulations and help to draft the manuscript. Shuangfang Lu defined (supervisor in China) the statement of problem. Chris Greenwell provide the main idea and help to draft the manuscript. Shuangfang Lu, Haitao Xue (vice supervisor in China), Chris Greenwell (supervisor in United Kingdom) designed and supervised the project. Tom Underwood help to discuss the main idea, provide the mineral model in the simulations and draft the manuscript. Fang Zeng, Guohui Chen, Chunzheng Wu and Rixin Zhao processed data and plotted figures. All authors reviewed the manuscript.

References

- (1) Bowker, K. A. *AAPG Bulletin*. **2007**, 91, 523-533.
- (2) Jarvie, D. M.; Hill, R. J.; Ruble, T. E.; Pollastro, R. M. *AAPG Bulletin*. **2007**, 91, 475-499.
- (3) Ross, D. J. K.; Bustin, R. M. *AAPG Bulletin*. **2008**, 92, 87-125.
- (4) Zou, C.N.; Dong, D. Z.; Wang, S. J.; Li, J. Z.; Li, X. J.; Wang, Y.; Li, D. H.; Cheng, K. M. *Petroleum Exploration and Development*. **2010**, 37 (6), pp. 641-653.
- (5) Brian, H.; Schulz, H. M. *Marine and Petroleum Geology*. **2012**, 31, 1-2.
- (6) Kinley, T. J.; Cook, L. W.; Breyer, J. A.; Jarvie, D. M.; Busbey, A. B. *AAPG Bulletin*. **2008**, 92, 967-991.
- (7) Kuhn, P. P.; Primio, R. di.; Hill, R.; Lawrence, J. R.; Horsfield, B. *AAPG Bulletin*. **2012**, 96, 1867-1897.
- (8) Kirschbaum, M. A.; Mercier, T. J. *AAPG Bulletin*. **2013**, 97, 899-921.
- (9) EIA, *Energy Information Administration*. 2016, (https://www.eia.gov/energy_in_brief/article/shale_in_the_united_states.cfm).
- (10) L. Doman, *Energy Information Administration*. 2016, (<http://www.eia.gov/todayinenergy/detail.cfm?id=26352>).
- (11) EIA, **2013**, (<http://www.eia.gov/pressroom/presentations>).
- (12) Zhang, L.; Bao, Y.; Li, J.; Li, Z.; Zhu, R.; Zhang, J. *Petrol. Explor. Develop.* **2014**, 41 (6), 703-711.
- (13) Zou, C.; Yang, Z.; Zhang, G.; Hou, L.; Zhu, R.; Tao, S.; Yuan, X.; Dong, D.; Wang, Y.; Guo, Q.; Wang, L.; Bi, H.; Li, D.; Wu, N. *Petrol. Explor. Develop.* **2014**, 41 (1), 14-30.
- (14) EIA, 2015, (<http://www.eia.gov/analysis/studies/worldshalegas/>).
- (15) Jia, C. Z.; Zheng, M.; Zhang, Y. F. *Acta Petrolei Sinica*. **2014**, 35, 1-10.
- (16) Zou, C. N.; Zhai, G. M.; Zhang, G. Y.; Wang, H. J.; Zhang, G. S.; Li, J. Z.; Wang, Z. M.; Wen, Z. X.; Ma, F. *Petroleum Exploration and Development*. **2015**, 42 (1), 1-13.
- (17) Nelson, P. H. *AAPG Bull*, **2009**, 93, 329-340.
- (18) Zou, C.; Yang, Z.; Cui, J.; Zhu, R.; Hou, L.; Tao, S.; Yuan, X.; Wu, S.; Lin, S.; Wang, L.; Bai, B.; Yao, J. *Petrol. Explor. Develop.* **2013**, 40 (1), 15-27.
- (19) Tang, X.; Zhang, J.; Wang, X. *Int. J. Coal Geol.* **2014**, 128-129, 32-46.
- (20) McGonigal, G.C.; Bernhardt, R. H.; Thomson, D. J. *Appl. Phys. Lett.* **1990**, 57, 28-30.
- (21) Castro, M. A.; Clarke, S. M.; Inaba, A.; Dong, C. C.; Thomas, R. K. *J. Phys. Chem. B*. **1998**, 102 (51), 10528-10534.
- (22) Severson, B. L.; Snurr, R. Q. *J. Chem. Phys.* **2007**, 126, 134708.
- (23) Harrison, A.; Cracknell, R. F.; Krueger-Venus, J.; Sarkisov, L. *Adsorption*, **2014**, 20, 427-437.
- (24) Ambrose, R. J.; Hartman, R. C.; Akkutlu, I. Y. *Society of Petroleum Engineers*. **2011**, SPE-141416-MS, Oklahoma City.
- (25) Ambrose, R. J.; Hartman, R. C.; Diaz-Campos, M.; Akkutlu, I. Y.; Sondergeld, C. H. *Society of Petroleum Engineers*. **2012**, 17, 219-229.
- (26) Hartman, R. C.; Ambrose, R. J.; Akkutlu, I. Y.; Clarkson, C. R. *Society of Petroleum Engineers*. **2011**, SPE-144097-MS, Woodlands, TX.
- (27) Wang, S.; Feng, Q.; Javadpour, F.; Xia, T.; Li, Z. *International Journal of Coal Geology*. **2015**, 147, 9-24.

- (28) Zhong, J.; Wang, P.; Zhang, Y.; Yan, Y.; Hu, S.; Zhang, J. *Energy*. **2013**, 59, 295–300.
- (29) Wu, G.; He, L.; Chen, D. *Chemosphere*. **2013**, 92, 1465–1471.
- (30) Xiong, Y.; Cao, T.; Chen, Q.; Li, Z.; Yang, Y.; Xu, S.; Yuan, S.; Sjoblom, J.; Xu, Z. *The Journal of Physical Chemistry C*. **2017**, 121(9), 5020–5028.
- (31) Lu, G.; Zhang, X.; Shao, C.; Yang, H. *Petroleum Science*. **2009**, 6, 76–81.
- (32) Underwood, T.; Erastova, V.; Cubillas, P.; Greenwell, H.C. *Journal of physical chemistry C*. **2015**, 119(13), 7282–7294.
- (33) Underwood, T.; Erastova, V.; Greenwell, H.C. *Journal of Physical Chemistry C*. **2016**, 120(21): 11433–11449.
- (34) Li, X.; Bai, Y.; Sui, H.; He, L. *Energy & Fuels*. **2017**, 31(2), 1174–1181.
- (35) Wilson, M. J. *Clay Minerals*. **1999**, 34, 7–25.
- (36) van Duin, A.C.; Larter, S.R. *Organic Geochemistry*. **2001**, 32, 143–150.
- (37) Hu, X.L.; Michaelides, A. *Surface Science*. **2008**, 602, 960–974.
- (38) Johnson, E.R.; Otero-de-la-Roza, A. *Journal of chemical theory and computation*. **2012**, 8(12), 5124–5131.
- (39) Fafard, J.; Lyubimova, O.; Stoyanov, S.R.; Dedzo, G.K.; Gusarov, S.; Kovalenko, A. *The Journal of Physical Chemistry C*. **2013**, 117(36), 18556–18566.
- (40) Huang, W.; Dedzo, G.K.; Stoyanov, S.R.; Lyubimova, O.; Gusarov, S.; Singh, S.; Lao, H.; Kovalenko, A.; Detellier, C. *The Journal of Physical Chemistry C*. **2014**, 118(41), 23821–23834.
- (41) Lage, M.R.; Stoyanov, S.R.; Carneiro, J.W. de M.; Dabros, T.; Kovalenko, A. *Energy&Fuels*. **2015**, 29(5), 2853–2863.
- (42) Greathouse, J.A.; Pike, D.Q.; Greenwell, H.C.; Johnston, C.T.; Wilcox, J.; Cygan, R.T. *Clays and Clay Minerals*. **2015**, 63, 185–198.
- (43) Pourmohammadbagher, A.; Shaw, J.M. *Energy&Fuels*. **2016**, 30(8), 6561–6569.
- (44) Fazelabdolabadi, B.; Alizadeh-Mojarad, A. *Applied Nanoscience*. **2017**, 1–11.
- (45) Downs, R. T.; Hall-Wallace, M. *Am. Mineral*. **2003**, 88, 247–250.
- (46) Bish, D. L. *Clays Clay Miner*. **1993**, 41, 738–744.
- (47) Curtis, M.E.; Cardott, B.J.; Sondergeld, C.H.; Raia, C.S. *International Journal of Coal Geology*, **2012**, 103, 26-31.
- (48) Li, J.J.; Yin, J.X.; Zhang, Y.N.; Lu, S.F. *International Journal of Coal Geology*, **2015**, 152, 39-49.
- (49) Sposito, G. *The Chemistry of Soils*. Oxford University Press: New York, **2008**.
- (50) Geatches, D.L.; Greenwell, H.C.; Clark, S.J. *J. Phys. Chem. A*. **2011**, 115, 2658-2667.
- (51) Newman, S.P.; Greenwell, H.C.; Coveney, P.V.; Jones, W. *J. Mol. Structure*. **2003**, 647, 1-3, 75.
- (52) Martínez, L.; Andrade, R.; Birgin, E. G.; Martínez, J. M. *J. Comput. Chem*. **2009**, 30, 2157–2164.
- (53) Cygan, R. T.; Liang, J. J.; Kalinichev, A. G. *J. Phys. Chem. B*. **2004**, 108 (4), 1255–1266.
- (54) Vanommeslaeghe, K.; Hatcher, E.; Acharya, C.; Kundu, S.; Zhong, S.; Shim, J.; Darian, E.; Guvench, O.; Lopes, P.; Vorobyov, I. *J. Comput. Chem*. **2010**, 31 (4), 671–690.

- (55) Bjelkmar, P.; Larsson, P.; Cuendet, M. A.; Hess, B.; Lindahl, E. *J. Chem. Theory Comput.* **2010**, 6 (2), 459–466.
- (56) Pastor, R. W.; MacKerell Jr, A. D. *J. Phys. Chem. Lett.* **2011**, 2 (13), 1526–1532.
- (57) Wright, L. B.; Walsh, T. R. *J. Chem. Phys.* **2012**, 137, 224702.
- (58) Skelton, A.; Fenter, P.; Kubicki, J. D.; Wesolowski, D. J.; Cummings, P. T. *J. Phys. Chem. C.* **2011**, 115 (5), 2076–2088.
- (59) Hess, B.; Kutzner, C.; van der Spoel, D.; Lindahl, E. *J. Chem. Theory Comput.* **2008**, 4 (3), 435–447.
- (60) Pronk, S.; Páll, S.; Schulz, R.; Larsson, P.; Bjelkmar, P.; Apostolov, R.; Shirts, M. R.; Smith, J. C.; Kasson, P. M.; van der Spoel, D. *Bioinformatics.* **2013**, 29, 845–854.
- (61) Zhou, Y. S.; Littke, R. *Marine and Petroleum Geology.* **1999**, 16, 771–792.
- (62) Humphrey, W.; Dalke, A.; Schulten, K. *J. Mol. Graphics.* **1996**, 14, 33–38.
- (63) Sha, M.; Zhang, F.; Wu, G.; Fang, H.; Wang, C.; Chen, S.; Zhang, Y.; Hu, J. *J. Chem. Phys.* **2008**, 128 (13), 134504.
- (64) Do, D. D.; Do, H. D. *Chem. Eng. Sci.* **2005**, 60, 1977–1986.
- (65) Severson, B. L.; Snurr, R. Q. *Chem. Phys.* **2007**, 126, 134708.
- (66) Sha, M.; Zhang, F.; Wu, G.; Fang, H.; Wang, C.; Chen, S.; Zhang, Y.; Hu, J. *Chem. Phys.* **2008**, 128, 134504.
- (67) Davidchack, R.L.; Laird, B.B.; Roth, R. *Cond matter phys.* **2016**, 19 (2), 1-10.
- (68) Christenson, H. K.; Gruen, D. W. R.; Horn, R. G.; Israelachvili, J. N. *Chem. Phys.* **1987**, 87 (3), 1834–1841.
- (69) Dirand, M., Bouroukba, M., Chevallier, V., Petitjean, D., Behar, E., and Ruffier-Meray, V. *Journal of Chemical & Engineering Data.* **2002**, 47(2):115–143.
- (70) Chen, G., Lu, S., Zhang, J., Xue, Q., Han, T., Xue, H., Tian, S., Li, J., Xu, C., Pervukhina, M. *Fuels.* **2017**, 199, 14–21.
- (71) Kareem, R.M.A., Cubillas, P., Gluyas, J., Bowen, L., Hillier, S. and Greenwell, H.C. *J. Petrol. Sci. Eng.* **2017**, 149, 436–455.